
Evolution of Near-Sun Solar Wind Turbulence

P.K. Manoharan

Radio Astronomy Centre, National Centre for Radio Astrophysics,
Tata Institute of Fundamental Research, Udhagamandalam (Ooty), India

Summary. This paper presents a preliminary analysis of the turbulence spectrum of the solar wind in the near-Sun region $R < 50R_{\odot}$, obtained from interplanetary scintillation measurements with the Ooty Radio Telescope at 327 MHz. The results clearly show that the scintillation is dominated by density irregularities of size about 100 – 500 km. The scintillation at the small-scale side of the spectrum, although significantly less in magnitude, has a flatter spectrum than the larger-scale dominant part. Furthermore, the spectral power contained in the flatter portion rapidly increases closer to the Sun. These results on the turbulence spectrum for $R < 50R_{\odot}$ quantify the evidence for radial evolution of the small-scale fluctuations (≤ 50 km) generated by Alfvén waves.

1 Introduction

The solar wind is highly variable and inhomogeneous, and exhibits fluctuations over a wide range of spatial and temporal scales. The properties of these fluctuations, as they move outward in the solar corona, are controlled by the presence of both waves and turbulence (e.g., Coleman 1968, Belcher & Davis 1971). However, their relative contributions to the heating and acceleration of the solar wind have yet to be assessed fully (Tu & Marsch 1995, Harmon & Coles 2005).

Radio scattering and scintillation experiments measure density fluctuations, which are related to the wave field, density fluctuations, and magnetic turbulence (e.g., Higdon 1986, Montgomery et al. 1987). The density fluctuation spectrum roughly follows a Kolmogorov power law in the spatial scale range 100 – 1000 km, at distances well outside the solar wind acceleration region. However, nearer to the Sun the spectrum tends to be flat (e.g., Woo & Armstrong 1979). The spectrum of the high-speed streams from coronal holes is steeper than Kolmogorov decay, which is attributed to dissipation at scales above 100 km (e.g., Manoharan et al. 1994, 2000). There is considerable interest to understand the radial change of the fluctuations due to both waves and turbulence in the solar wind acceleration region. In this

study, spectral features are analysed over a range of distances from the Sun using interplanetary scintillation measurements made with the Ooty Radio Telescope at 327 MHz (Swarup et al. 1971).

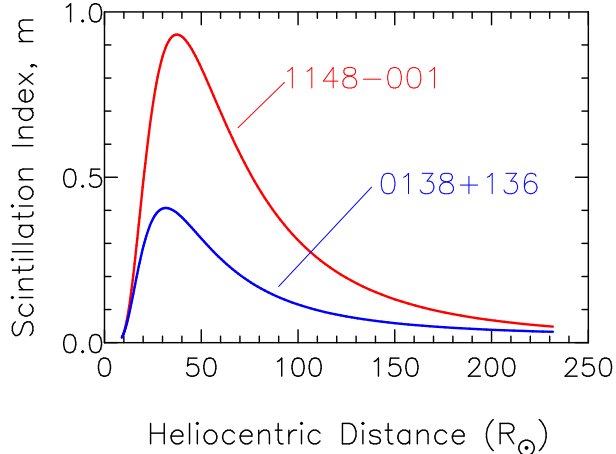


Fig. 1. Average scintillation index against heliocentric distance observed at 327 MHz. Radio quasars 1148-001 and 0138+136 have equivalent angular diameters of about 15 and 50 milli-arcsec, respectively.

2 Interplanetary scintillation

Interplanetary scintillation (IPS) is the variability of distant compact radio source (e.g., a quasar or a radio galaxy) caused by microturbulence in the solar wind of spatial scales 10 to 1000 km (e.g., Manoharan et al. 1994). Scintillation measurements normally refer to the instantaneous departure of intensity ($\delta I(t)$) from the mean intensity of the source ($\langle I \rangle$), i.e., $\delta I(t) = I(t) - \langle I \rangle$. Since the irregularities are convected by the solar wind, the statistical fluctuations of $\delta I(t)$ can be used to estimate the speed and turbulence spectrum of the solar wind, integrated along the line of sight to the radio source. However, for a given line of sight, the spectrum of scintillation drops rapidly with distance from the Sun, $C_N^2(R) \sim R^{-4}$, and the scattering is therefore concentrated where the line-of-sight is closest to the Sun. The shape of the turbulence spectrum can be inferred from the temporal IPS spectrum, obtained by taking the Fourier transformation of intensity time series. The rms intensity variation $\langle \delta I(t)^2 \rangle^{1/2}$ is the integral of the power spectrum. The scintillation index, m , is estimated by

$$m^2 = \frac{1}{\langle I \rangle^2} \int_0^{f_c} P(f) df, \quad (1)$$

where f_c is the cutoff frequency of the spectrum at which the scintillation equals the noise level. The systematic radial variation of $C_N^2(R)$ can be obtained from the index versus distance ($m - R$) plots as in Fig. 1. These smoothed plots represent average scintillations observed over several years for two well-known radio quasars (Manoharan 2008).

At given heliocentric distance, a compact source scintillates more than an extended one, because Fresnel filtering plays a key role in producing the intensity fluctuations and the scintillation is heavily attenuated by a large angular size $\theta \geq \sqrt{\lambda/Z}$, where λ is the wavelength of observation and Z is the distance to the scattering screen. The observations reported in this study have been made with the Ooty Radio Telescope (ORT), which operates at $\lambda=0.92$ m. In the case of near-Sun IPS measurements, the scattering medium is located at about 1 AU and therefore sources having angular size $\theta > 500$ milli-arcsec do not scintillate.

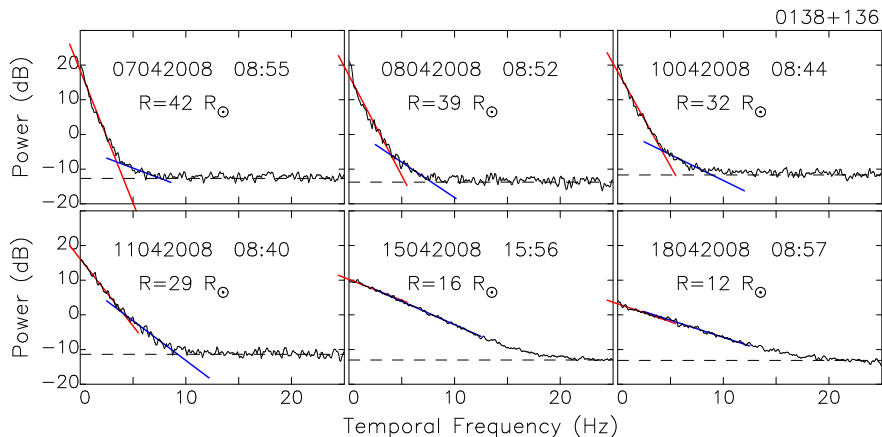


Fig. 2. Sample temporal power spectra of 0138+136 on log-linear scale, showing spectral shape variations with distance from the Sun. The date and time of observation and the heliocentric distance (R) are specified. These observations have been made at the eastern limb of the Sun so that the source approaches the Sun with increasing day number.

Figure 1 shows that as the Sun is approached, the scintillation increases to a peak value at a distance of $R \approx 40R_\odot$, and then decreases for further closer solar offsets (e.g., Manoharan 1993), where 1 solar radius is $R_\odot = 6.96 \times 10^5$ km. The peak or transition distance, $R \approx 40R_\odot$, is the characteristic of IPS measurement at $\lambda=0.92$ m. It is a function of observing wavelength and moves close to the Sun with decreasing wavelength (e.g., Coles 1978, Kolosov et al. 1982). At $R < 40R_\odot$, the scintillation index of an ideal point source saturates at $m \approx 1$. In the weak-scattering region with $R \geq 40R_\odot$, the decline in scintillation corresponds to a fall of turbulence approximately as $1/R^2$. The

shape of the temporal spectrum of the intensity fluctuations, $P(f)$, is linearly related to the spatial turbulence spectrum, $\Phi_{N_e}(q)$, which can be obtained by fitting the measured scintillation spectrum (Manoharan & Ananthakrishnan 1990, Manoharan et al. 1994). The turbulence spectrum is given by the power-law form $\Phi_{N_e}(q) \sim q^{-\alpha}$, with the power index α varying between 3 and 3.8, depending on the solar-wind source location on the Sun. The spatial spectrum also includes Gaussian cutoffs at high spatial wavenumber q , set by the source-size visibility and the inner (dissipation) scale of the solar wind turbulence.

3 Scintillation spectrum near the Sun

In the strong-scattering region with $R < 40R_\odot$, the turbulence is too intense and the relationship between the scintillation index and $C_N^2(R)$ takes a complex form. The decrease in scintillation is due to the smearing of scintillation caused by the angular size of the radio source. In a physical sense, many independent random secondary sources exist inside the Fresnel zone, reduce the coherence, and cause reduction of the intensity fluctuations. However, the strong-scintillation spectrum is wider than the weak case, and contains information on a large range of turbulence scales. The present study reports a systematic analysis of intensity scintillation measurements of compact radio sources ($\Theta \approx 50$ milli-arcsec) made with the ORT at 327 MHz. It allows to probe the solar wind from about 10 to $250R_\odot$. The closest solar offset is mainly limited by the ORT beam width. Figures 2 and 3 display temporal scintillation spectra of radio quasars 0138+136 and 0202+149, observed at different solar offsets during April 2008. The sampling rate, 50 Hz, employed in the present study in principle extends the temporal frequency range of the spectrum to 25 Hz, which allows to infer the statistics of even small-scale turbulence. For example, for a typical value of the solar wind speed V , the spectrum can cover spatial wavenumbers in the range $0.002 < q = (2\pi f/V) < 0.2 \text{ km}^{-1}$, corresponding to scales in the range 5 to 500 km.

Nearer to the Sun the spectrum broadens, suggesting systematic increase in turbulence associated with small-scale irregularity structures (< 100 km). The flattening of the spectrum at $R < 40R_\odot$ indicates addition of small-scale turbulence. The remarkable change is that the high-frequency part of the spectrum gradually extends into the low-frequency part at distances closer than the transition point ($R < 40R_\odot$). The diminishing of spectral power at scales close to the Fresnel radius suggests the possibility of dominant effect of Fresnel filter, which can smear the scintillation. At $R > 40R_\odot$, the low-frequency part of the spectrum gradually steepens and merges with the slope of the density turbulence spectrum at scales smaller than the Fresnel radius. When a large number of spectra on a given radio source, observed on consecutive days over a period of 45 days, are displayed in movie mode this gives a direct visualization, making the above results immediately apparent.

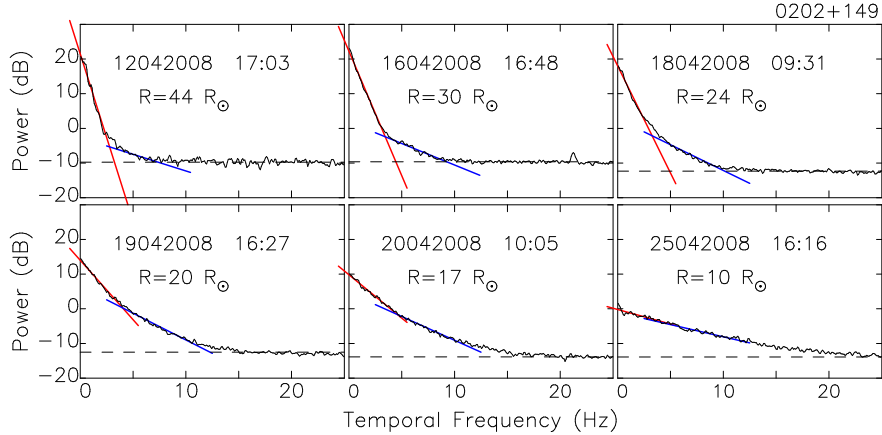


Fig. 3. Same as Fig. 2, for radio source 0202+149.

4 Radial evolution of small- and large-scale turbulence

Figure 4 shows the power of turbulence associated with the low- and high-frequency portions of the spectrum at different solar offsets for radio sources 0138+136 and 0202+149. These plots illustrate the attenuation and enhancement of the scintillations, respectively, for the large-scale (> 100 km) and the small-scale (< 100 km) spectral regions and their radial variations. For most of the temporal spectra, the slope change from high- to low-frequency part is apparent, and whenever the spectrum monotonously increases towards the low frequency part, the half-value of the cutoff frequency (i.e., $f_c/2$) is considered to mark the separation of the scintillation between the low- and high-frequency parts.

It is obvious that the turbulence density associated with the low-frequency part is dominant at all heliocentric distances and that it closely follows the shape of the overall scintillation index versus distance curve (Fig. 1). Manoharan (1993) has shown that the scintillation variation at $R > 40R_\odot$ is of power-law form, with $m \sim R^{-\beta}$ and $\beta = 1.7 \pm 0.2$. When the integration is accounted for, the scattering power changes as $C_N^2(R) \sim R^{-(2\beta+1)} = R^{-4.4 \pm 0.4}$. The scintillation in the low-frequency part of the spectrum is consistent with the above radial evolution. However, in the high-frequency part, the scintillation increases with decreasing solar offsets and tends to merge with the above portion. In the distance range $R = 15 - 100R_\odot$, the scintillation due to the high-frequency part follows the power-law $m_{\text{high_freq}} \sim R^{-b}$. Both sources show similar slopes $b \approx 2.0$ and 2.3 . However, the average radial trend is much steeper, with $C_{N_{\text{high_freq}}}^2(R) \sim R^{-(2b+1)} = R^{-5.3}$, than the density turbulence slope $\sim R^{-4}$. The turbulence associated with small-scale fluctuations (≤ 50 km) in the solar wind acceleration region steeply increases towards the Sun.

The strong scintillation spectra of selected radio sources observed at Ooty have also been compared with same-day observations at higher observing frequencies, for which the measurements fall in the weak scintillation regime. For example, IPS measurements with the Giant Metrewave Radio Telescope (GMRT) at 610 MHz (Manoharan et al., in preparation) and the European Incoherent Scatter (EISCAT) system at 931 MHz (R.A. Fallows, private communication) reveal spectral features that are closely similar to that observed with the ORT at low and high temporal frequencies. The contributions of low and high spatial scales of the scintillation spectrum are not altered in the transition from strong to weak scintillation.

5 Discussion and conclusion

Several IPS experiments have shown the turbulence spectrum to be $\Phi_{N_e} \sim q^{-\alpha}$, with the dissipative scale (i.e., inner scale or cutoff scale) size increasing linearly with distance as $l_i \approx (R/R_\odot)^{1\pm 0.1}$ km at $R \leq 100R_\odot$ (Manoharan et al. 1987, Coles & Harmon 1989, Manoharan et al. 1994). Further, a flatter spectrum ($\alpha \leq 3$) and smaller dissipative scales ($l_i < 10$ km) have been observed in the near-Sun solar wind acceleration region ($R < 20R_\odot$) (Coles & Harmon 1989, Yakovlev et al. 1980, Yamauchi et al. 1998). The present result of flatter spectrum for the low-frequency part, which at larger distances merges with the density turbulence spectrum, is consistent with the earlier findings.

The effects of the angular structure of the radio source and of inner-scale turbulence dissipation are three-dimensionally Gaussian in shape, and tend to attenuate the high-frequency tail of the spectrum (Manoharan et al. 1987, Yamauchi et al. 1998). The inner-scale contribution is not significant at small solar offsets (it decreases and becomes small at regions close to the Sun). Furthermore, the effect of the angular size of the compact radio source ($\Theta \approx 50$ milli-arcsec) is considerably small. However, the key point is that, in the near-Sun regions ($R < 40R_\odot$), a significant enhancement in scintillation power is measured at the high-frequency portion of the spectrum, well above the dissipation and source-size cutoff levels. In order to show scintillation above these cutoffs in the tail part of the spectrum, strong fluctuations are likely to be present which are oriented in different directions than the radial flow of the solar wind. Therefore, the systematic and significant increase in power at the small-scale part of the spectrum suggests an active role of irregularities produced by magnetosonic waves in the solar wind, with multiple scale sizes and vector directions. The rapid radial change of the turbulence associated with the small-scale irregularities, $C_{N(\text{high-freq})}^2(R) \sim R^{-5.3}$, indicates that the dominant contribution is due to wave-generated turbulence in the solar wind acceleration region. Therefore, the overall near-Sun turbulence spectrum can be explained by the combined effects of the smeared density turbulence

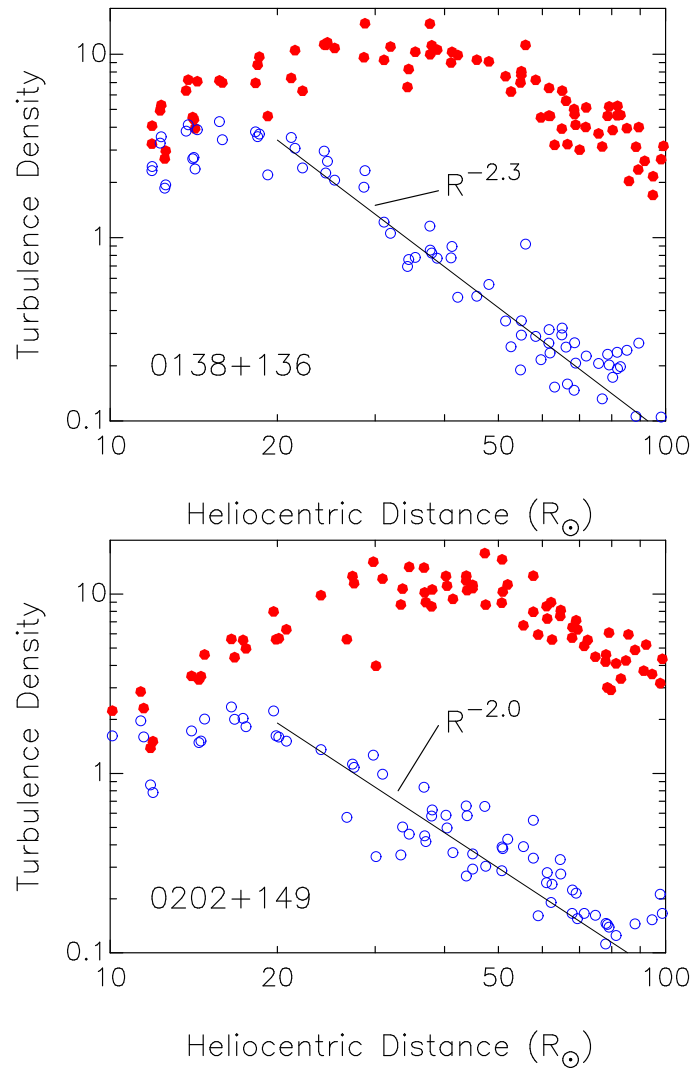


Fig. 4. Radial turbulence evolution in the low-frequency (*filled symbols*) and high-frequency portions (*open symbols*) of the spectrum.

spectrum and the strong fluctuations generated by Alfvén waves at small scales (≤ 50 km).

In summary, this preliminary analysis of the temporal spectrum of scintillations measured in the solar wind acceleration region provides evidence that, apart from density turbulence, small-scale fluctuations produced by magnetosonic waves plays a key role in shaping the spectrum. In comparison with the density turbulence, the effect of waves is significant but its importance

decreases rather steeply with heliocentric distance. Its presence in the solar wind extends outside the acceleration region ($R > 20R_{\odot}$), although weaker in intensity. A more rigorous study of the small-scale microturbulence, its variation with the solar cycle and solar source regions will be reported in more detail elsewhere.

Acknowledgement. The author thanks the observing/engineering team and research students of the Radio Astronomy Centre for help in performing the observations and the preliminary data reduction. This work is partially supported by the CAWSES-India Program, which is sponsored by the Indian Space Research Organisation (ISRO).

References

- Belcher, J. W., Davis, Jr., L. 1971, JGR, 76, 3534
 Coleman, Jr., P. J. 1968, ApJ, 153, 371
 Coles, W. A. 1978, Space Sci. Rev., 21, 411
 Coles, W. A., Harmon, J. K. 1989, ApJ, 337, 1023
 Harmon, J. K., Coles, W. A. 2005, JGR, 110, 3101
 Higdon, J. C. 1986, ApJ, 309, 342
 Kolosov, M. A., Yakovlev, O. I., Efimov, A. I., et al. 1982, Radio Sci., 17, 664
 Manoharan, P. K. 1993, Solar Phys., 148, 153
 Manoharan, P. K. 2008, The Solar Wind (Princeton Series in Astrophysics), 235–266
 Manoharan, P. K., Ananthakrishnan, S. 1990, MNRAS, 244, 691
 Manoharan, P. K., Ananthakrishnan, S., Pramesh Rao, A. 1987, in Sixth International Solar Wind Conference, eds. V. J. Pizzo, T. Holzer, & D. G. Sime, 55
 Manoharan, P. K., Kojima, M., Gopalswamy, N., Kondo, T., Smith, Z. 2000, ApJ, 530, 1061
 Manoharan, P. K., Kojima, M., Misawa, H. 1994, JGR, 99, 23411
 Montgomery, D., Brown, M. R., Matthaeus, W. H. 1987, JGR, 92, 282
 Swarup, G., Sarma, N. V. G., Joshi, M. N., et al. 1971, Nat, 230, 185
 Tu, C.-Y., Marsch, E. 1995, Space Sci. Rev., 73, 1
 Woo, R., Armstrong, J. W. 1979, JGR, 84, 7288
 Yakovlev, O. I., Efimov, A. I., Razmanov, V. M., Shtrykov, V. K. 1980, Soviet Ast., 24, 454
 Yamauchi, Y., Tokumaru, M., Kojima, M., Manoharan, P. K., Esser, R. 1998, JGR, 103, 6571